NANO LETTERS

pubs.acs.org/NanoLett Letter

All-Optical Valley Polarization Switch via Controlling Spin-Triplet and Spin-Singlet Interlayer Exciton Emission in WS_2/WSe_2 Heterostructure

Yue Hu, Xinglin Wen,* Jiamin Lin, Wendian Yao, Yingying Chen, Junze Li, Sijie Chen, Lei Wang, Weigao Xu, and Dehui Li*

Cite This: *Nano Lett.* 2023, 23, 6581−6587 Read Online

ACCESS | Metrics & More | Article Recommendations | Supporting Information

ABSTRACT: Although selective singlet and triplet interlayer exciton (IX) emission of transition metal dichalcogenides (TMD) heterostructures can be achieved by applying an electric or magnetic field, the device structure is complex and a low temperature is usually required. Here, we demonstrate a simple all-optical approach to selectively enhance the emission of singlet and triplet IX by selectively coupling singlet or triplet IX of a WS_2/WSe_2 heterostructure to a SiO_2 microsphere cavity. Angle-resolved photoluminescene reveals that the transition dipole of triplet IX is almost along the out-of-plane direction, while singlet IX only has 69% out-of-plane dipole moment contribution. Since the out-of-plane dipole presents a higher Purcell factor within the cavity, we can simultaneously enhance the emission intensity of IX and control the emissive IX species at room temperature in an all-optical route. Importantly, we demonstrate an all-optical valley polarization switch with a record high on/off ratio of 35.

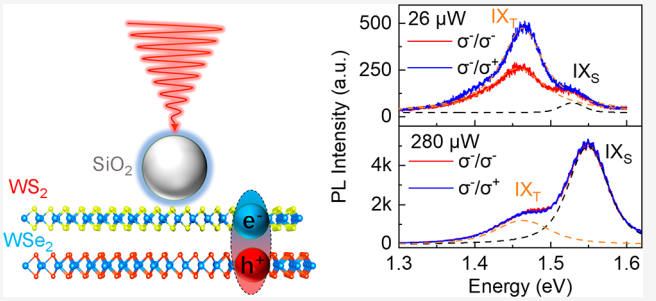

KEYWORDS: *Transition metal dichalcogenides, heterostructures, interlayer exciton, SiO_2 cavity, valley polarization switch*

Transition metal dichalcogenide (TMD) van der Waals (vdW) heterostructures with type-II band alignment enable the generation of interlayer exciton (IX), where electrons and holes reside in separated layers.[1−4] The spatial separation between electrons and holes gives rise to a long lifetime in the order of hundreds of nanoseconds,[5−7] which is beneficial to valleytronic devices. In addition, the electronic band hybridization and strong spin−orbit coupling lead to the unique spin-valley physics in TMD heterostructures.[8−10] Spin-singlet (IX_S) and spin-triplet (IX_T) interlayer excitons have opposite spin orientation, making them useful in valley switch and valley logic devices.[11,12] In contrast to the scenario of monolayer TMDs in which only intralayer excitons with in-plane (IP) dipole moment are transition allowed,[13] theoretical calculations and experimental demonstrations validate that IX_S and IX_T in the heterostructure exhibit comparable coupling strength with in-plane and out-of-plane (OP) polarized light depending on the atomic registry.[14−17] In other words, the transition dipole moment of IX can be IP orientated although they have permanent OP electric dipole moment.[14]

The modified selection rule of IX in heterostructure offers opportunities to construct a valley polarization switch by selectively exciting IX_S and IX_T. However, most of the previous work used the electric field induced Stark effect or magnetic field induced Zeeman effect to observe fine structures of IX.[11,18−20] For instance, Ciarrocchi et al. utilized the electrostatic doping effect and the quantum confined Stark effect simultaneously to regulate the spin−orbit coupling of IX at the temperature of 4.2 K.[12] They also realized interlayer exciton Zeeman splitting by the magneto-induced Zeeman effect on the same sample.[12] Although previous works have observed and controlled IX_S and IX_T fine structures, complex device structures and harsh experimental conditions such as large electric/magnetic field and low temperatures impose limitations on practical applications.

Here we report an all-optical approach to selectively control IX_S and IX_T emission and their valley polarization by coupling tungsten diselenide (WSe_2)/tungsten disulfide (WS_2) vdW heterojunctions to a SiO_2 cavity. The SiO_2 microsphere cavity prefers to enhance the IX_T emission since the IX_T transition dipole has a larger component in the OP direction. The polarization-resolved momentum-space emission measurement indicates that IX_T has 92% OP dipole moment contribution, while the IX_S dipole only has 69% OP component. By utilizing

Received: May 8, 2023
Revised: July 10, 2023
Published: July 13, 2023

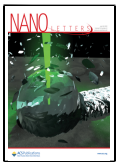

https://doi.org/10.1021/acs.nanolett.3c01698
Nano Lett. 2023, 23, 6581−6587

the selective emission of IX_S and IX_T, we realize a valley polarization switch with an on/off ratio of 35 in an all-optical route. These marvelous optical properties pave the way for the development of all-optical valleytronics devices.

Figure 1a displays a schematic illustration of our device in which a SiO_2 cavity is placed on the top of the WSe_2/WS_2 heterostructure. Figure 1b exhibits the optical microscopy image of a heterostructure device with the monolayer WSe_2, monolayer WS_2, and SiO_2 cavity highlighted by different colors of dashed lines. The inset of Figure 1b shows the scanning electron microscopy (SEM) image of a SiO_2 cavity with the diameter of 5 μm. Due to the effect of gravity and intermolecular forces, the SiO_2 cavity will adhere tightly to the surface of the heterostructure, preventing it from moving or rolling. The sphere was kept at a fixed position during our measurement. The photoluminescence (PL) spectra of WSe_2/WS_2 heterostructure under the 633 nm laser excitation were carried out on the position with (red curve) and without (blue curve) the SiO_2 cavity (Figure 1c). Both the intralayer exciton of monolayer WSe_2 and IX emission can be observed around the energy of 1.65 and1.42 eV,[21] respectively. It should be pointed out that the oscillations of intralayer exciton emission in the presence of SiO_2 cavity is caused by the resonance of the whispering gallery mode (WGM) of the cavity[22,23] (Figure S1, Supporting Information). Strong interlayer exciton emission and quenching of monolayer WSe_2 luminescence suggest that strong interlayer coupling is present. Significant IX enhancement can be observed in the presence of SiO_2 cavity with an average enhancement factor of 3, and the maximum magnification is around 7 times. More importantly, an obvious splitting of IX emission peak can be observed in the presence of SiO_2 cavity with the splitting energy around 50 meV, which is consistent with the WS_2 conduction band splitting.[24] Accordingly, we speculate that the IX peak splitting is caused by spin−orbit splitting of the WS_2 conduction band. We measured SHG of monolayer WS_2, WSe_2, and the heterostructure, as displayed in Figure S2. SHG of heterostructure is the coherent superposition of SHG of monolayer WS_2 and WSe_2 with phase difference determined by the twist angle. It is observed in our sample that SHG in the heterostructure region is enhanced compared with the monolayers, which indicates that the heterojunction is near 0° stacking (R-stacking).[25]

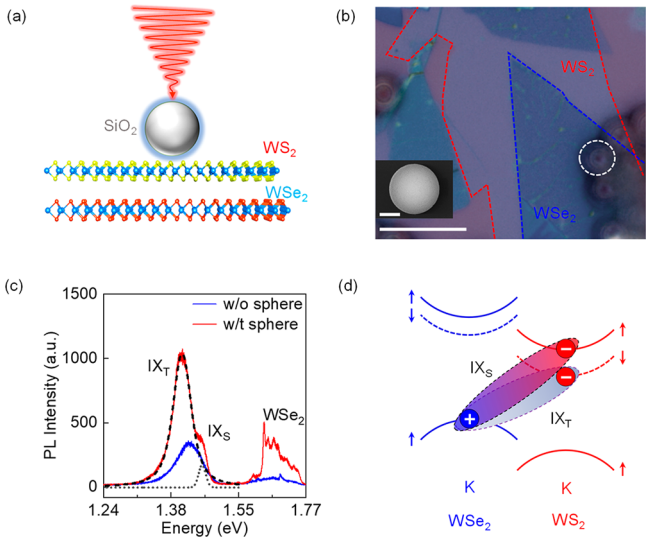

Figure 1. (a) Schematic illustration of the device structure. (b) Optical microscopy image of the fabricated device. SiO_2 cavity, monolayer WSe_2, and WS_2 flakes are highlighted by the white, blue and red dashed lines, respectively. The scale bar is 10 μm. The inset shows the scanning electron microscopy (SEM) image of a SiO_2 cavity with the scale bar of 2 μm. (c) PL spectra of the WSe_2/WS_2 heterostructure with (red line) and without (blue line) SiO_2 cavity on top. IX_S and IX_T donate the spin-singlet and spin-triplet interlayer excitons as fitted. (d) Band alignment of the heterostructure with R-stacking. The black and purple elliptical dashed lines show the formation of singlet and triplet interlayer excitons.

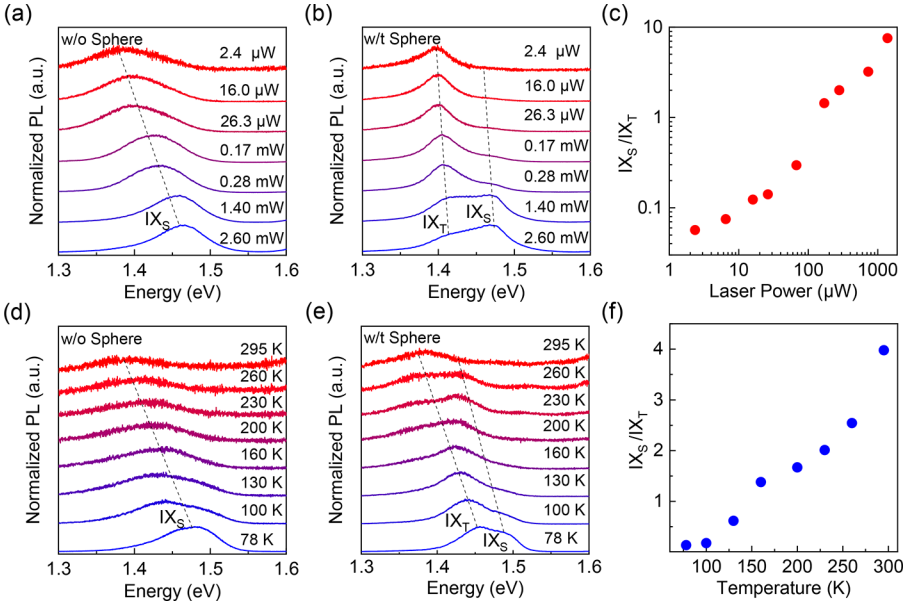

Figure 2. (a and b) Excitation power-dependent interlayer exciton PL spectra of the heterostructure without and with the SiO_2 cavity, respectively. (c) Excitation power-dependent emission intensity ratio of IX_S to IX_T for the heterostructure with SiO_2 cavity. (d and e) Temperature-dependent interlayer exciton PL spectra of the heterostructure without and with SiO_2 cavity, respectively. (f) Temperature-dependent emission intensity ratio of IX_S to IX_T for the heterostructure with SiO_2 cavity.

https://doi.org/10.1021/acs.nanolett.3c01698
Nano Lett. 2023, 23, 6581−6587

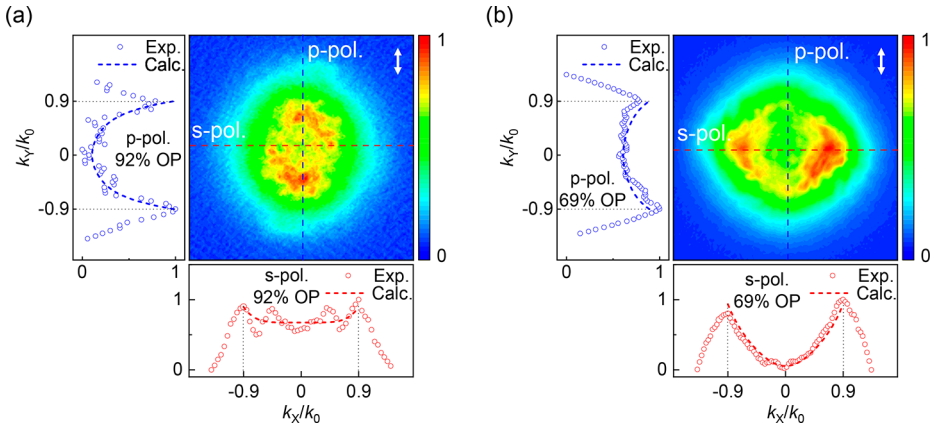

Figure 3. (a and b) Back focal plane images of IX_T and IX_S emission, respectively. The white arrow represents the polarization of excitation laser. The left and bottom panels in each picture are extracted p-polarized and s-polarized PL.

Figure 1d displays the band alignment of the heterostructure with R-stacking. Electrons in the high-energy spin-up and low-energy spin-down conduction band of WS_2 interact with the holes in the valence band of WSe_2 via Coulomb force to form spin-singlet IX (IX_S) and spin-triplet IX (IX_T), respectively.[26]

In order to verify the formation of IX_S and IX_T, we have carried out excitation power-dependent PL measurements of the heterostructure region without and with cavity, as shown in Figure 2a,b, respectively. The detailed curve fitting is displayed in Figure S3. Only one IX emission peak can be observed in the heterostructure region without a cavity (Figure 2a), which is normally assigned as IX_S according to a previous report.[27] The IX_S peak blue-shifts with the increase of the excitation power, which is attributed to the dipole−dipole repulsion at high exciton density.[28] In contrast, we can clearly observe two emission peaks in the energy range of 1.31−1.46 eV for the sample with cavity and both emission peaks blue shift with the excitation power, indicating both of them are interlayer excitons instead of intralayer excitons (Figure 2b). In addition, the energy difference of these two peaks remains 50 meV regardless of excitation power, suggesting they originate from IX_S and IX_T emission due to the intrinsic conduction band splitting of WS_2. The mechanism of the appearance of the additional IX_T peak for the sample with a SiO_2 cavity will be discussed later. The additional IX_T for the sample with SiO_2 cavity is also observed in the $WSe_2/MoSe_2$ heterostructure with splitting energy of 30 meV (Figure S4), which is consistent with the conduction band splitting of $MoSe_2$.[6] The similar results in different heterostructures indicate that the method to selectively enhance the IX_T emission is universal.

Figure 2c shows the extracted PL intensity ratio of IX_S to IX_T for the sample with SiO_2 cavity. The ratio increases with excitation power, indicating that IX_S dominates at high excitation power, while IX_T is much stronger under low-power excitation. Under high-power excitation, electrons are populated in the high-energy spin-conserving states, and thus, IX_S is dominant. In contrast, electrons mostly occupy the low-energy spin-flipping states under a low-power excitation, which results in the dominant IX_T.[6]

We have further performed temperature-dependent PL measurements on the heterojunction without and with a SiO_2 cavity as shown in Figure 2d,e, respectively. Both IX_S and IX_T can be observed even at room temperature for the heterostructure with the SiO_2 cavity (Figure 2e). In addition, as the temperature increases, IX_S and IX_T emission peaks show a redshift, which is a typical characteristic of interlayer exciton.[29] Figure 2f plots the extracted IX_S/IX_T ratio versus temperature, which suggests that IX_S becomes more obvious at higher temperature. Electrons in the spin-flipping conduction band are excited to the high-energy spin-conserving conduction band with increasing temperature, which is consistent with a previous report that IX_S emission will gradually become stronger with the increase of temperature.[30] The lifetimes of IX_S and IX_T are also measured as shown in Figure S5. For the heterostructure without a cavity, only IX_S can be detected with a lifetime of 1.9 ns. When coupling to a cavity, IX_S and IX_T exhibit lifetimes of 1.7 and 4.0 ns, respectively. The reduction of the lifetime of IX_S after coupling to the cavity is attributed to the Purcell effect induced by the cavity. The Purcell effect enhances the local density of states (LDOS) and the radiative recombination rate, resulting in declined lifetime of the exciton and thus an enhancement of PL intensity. The longer lifetime of IX_T compared with IX_S for the heterostructure with cavity is because of the additional spin-flipping process,[31] which agrees with our interpretation that the observed additional peak in Figure 1c is IX_T emission.

As shown in Figures 1c and 2b, the IX_T emission peak exhibits a much larger PL enhancement than IX_S in the presence of SiO_2 cavity. In order to further explore the coupling of IX_S and IX_T states to SiO_2 cavity, we conduct angle-resolved PL measurements at room temperature using an objective lens with a numerical aperture (NA) of 0.9 (Figure S6). Figure 3a,b displays the back focal plane (k-space) images of IX_T and IX_S emission, respectively. The white double arrows in the figures represent the excitation polarization while the red and blue dotted lines represent the s-polarized and p-polarized emission, respectively. The left and bottom panels are extracted p-polarized and s-polarized PL intensity. By fitting the s- and p-polarized PL,[32,33] we obtain that IX_T composes 92% OP dipole moment, while IX_S only has 69% OP dipole contribution. These results are consistent with previous theoretical studies and experimental reports that IX transition dipole can have both IP and OP components although the electric dipole is always along the OP direction.[14] It is worth noting that the angle-resolved PL in Figure 3 was measured at room temperature instead of low temperature. The dipole orientation is independent of temperature and room temperature is preferred for angle-resolved PL measurement in our experiment because an objective with large NA (0.9) is desired

https://doi.org/10.1021/acs.nanolett.3c01698
Nano Lett. 2023, 23, 6581−6587

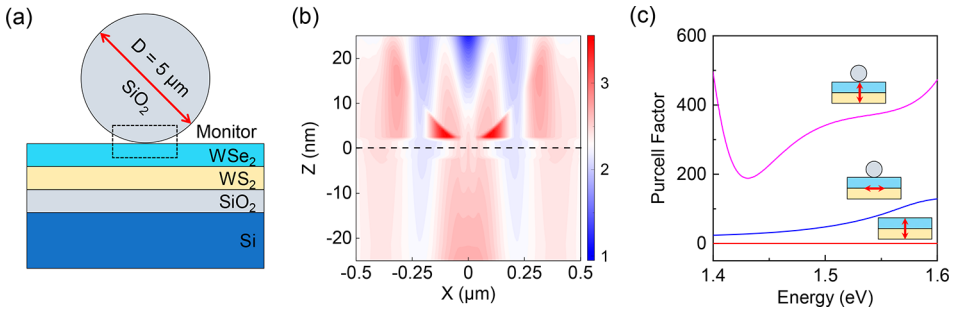

Figure 4. (a) Setting of the simulation structure. The black box represents the calculation area. (b) The electric field enhancement of the device with a SiO_2 cavity. (c) Purcell factor of the bare out-of-plane dipole (red), SiO_2 cavity-coupled in-plane (blue), and out-of-plane dipole (magenta).

to enhanced collection efficiency for the emission from the OP dipole.

The distinct dipole orientation of IX_S and IX_T will lead to different coupling strengths to the SiO_2 cavity. The Purcell factors are calculated via lumerical FDTD solutions to investigate the PL enhancement difference between IX_S and IX_T as shown in Figure 4. Figure 4a shows the cross-sectional view of the simulated structure, including a SiO_2 cavity with a diameter of 5 μm on the top of a monolayer WSe_2 and WS_2. A monitor with height of 50 nm and width of 1.2 μm is set to resolve the electric field distribution at the interface between the cavity and the TMDs. Noticeable electric field enhancement at the TMDs/cavity interface can be observed (Figure 4b) and the magnification of the electric field is around 3 times (Figure S7). Furthermore, we simulate the Purcell factor of the bare OP dipole and cavity-coupled IP and OP dipole emission in Figure 4c. The Purcell factor of the dipole emission of the sample without cavity is close to 1 because there is no electric field enhancement. Remarkably, the cavity-coupled OP dipole exhibits a much larger Purcell factor than the cavity-coupled IP dipole at the IX emission energy range (1.4−1.6 eV). To sum up, the IX_T transition dipole has a larger component in the OP direction (Figure 3) and thus leads to a larger Purcell enhancement when coupled to the SiO_2 cavity. The selective emission enhancement can render IX_T dominant over IX_S emission in the presence of a SiO_2 cavity.

According to the excitation power-dependent switch between IX_T and IX_S in the heterostructure with SiO_2 cavity, we design an all-optical spin singlet−triplet interlayer exciton switch in Figure 5a. It can be clearly seen that the low-energy IX_T emission peak dominates under an excitation power of 26 μW (red curve), while IX_S dominates when the excitation power increases to 280 μW (blue curve). Based on this, the switch between IX_T and IX_S can be readily achieved by varying the excitation power. The IX_T/IX_S ratio can be switched stably (Figure 5b). For comparison, we also test the IX_T and IX_S emission for the sample without SiO_2 cavity by switching the excitation power (Figure S8a), and only IX_S can be observed regardless of excitation power, which indicates that the SiO_2 cavity indeed enables the selective emission enhancement of IX_T.

IX_T and IX_S have opposite spin orientation, and the emission will present with distinct valley polarization depending on the local atomic registry.[14] Circularly polarized PL of the heterostructure is measured, as shown in Figure 5c. A negative degree of valley polarization (DOP = $\frac{I_{\sigma-} - I_{\sigma+}}{I_{\sigma-} + I_{\sigma+}}$) of −26% is resolved for IX_T peak under a 26 μW left-hand (σ-) polarized excitation, where $I_{\sigma-}$ and $I_{\sigma+}$ are the intensity of left- and right-hand circularly polarized emission. Figure 3c indicates that 92% of the IX_T dipole is z-polarized, which should exhibit zero valley polarization. However, the observed DOP of IX_T emission is larger than 8%. This is because each dipole with IP and OP moment has different contribution to the total PL due to the deviated quantum efficiency, collection efficiency, and scattering process. First, the quantum efficiencies of luminescence of IP and OP dipole are different as the calculation indicates.[34] In terms of R-stacking, the optical matrix elements (namely, quantum efficiency) of the IX_T dipole with the OP moment are lower than the IP moment. This discrepancy makes PL coming from IP dipole moment exceed 8%, although the amount of IP dipole only has 8% in proportion. Second, an objective with NA < 1 exhibits a higher collection efficiency for IP dipoles compared with OP dipoles because IP and OP dipole exhibit distinct radiation pattern spatially.[35] An objective with NA of 0.6 is used in our PL measurement, which leads to the contribution of IP dipole exceeding 8%. Finally, valley polarization could be observed for dark exciton with OP moment because of the scattering

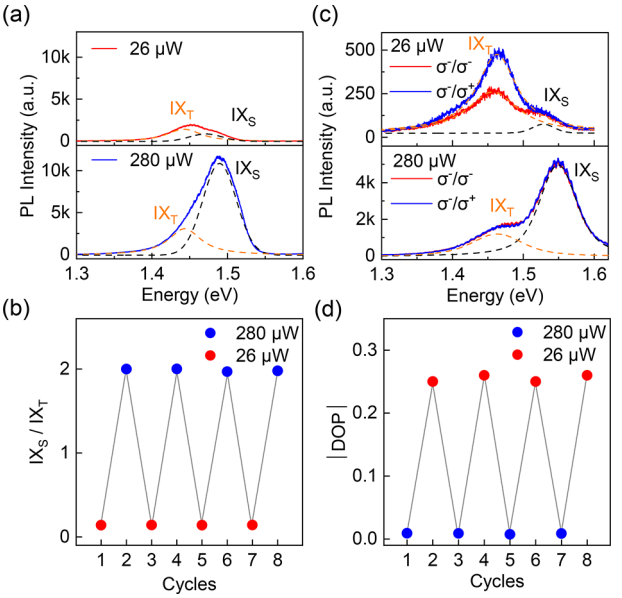

Figure 5. (a) IX emission of the heterostructure under excitation powers of 26 and 280 μW. (b) Cyclic test of the IX_S/IX_T emission intensity ratio. The red and blue dots indicate the IX_S/IX_T ratio under excitation powers of 26 and 280 μW, respectively. (c) Valley polarized emission of IX under excitation powers of 26 and 280 μW. (d) Cyclic test of the valley polarization switch. The red and blue dots indicate the valley degrees of IX_T emission under excitation powers of 26 and 280 μW, respectively.

https://doi.org/10.1021/acs.nanolett.3c01698
Nano Lett. 2023, 23, 6581−6587

process of bright (singlet) to dark (triplet) states according to the report by Tang et al.[36] We interpret that the valley polarization of the IX dipole with OP moment is possibly initiated by a scattering process similar to that in the literature.[36] Valley contrast PL was also measured under right-handed light excitation in Figure S9 with a DOP of 25%, which is close to the result under left-handed light excitation.

However, valley polarized emission is absent for IX_S emission. There are three kinds of atomic registry (R_h^M, R_h^h, and R_h^X) in R-stacking heterostructure, and all of them contribute to the IX emission. For singlet IX transition, R_h^M, R_h^h, and R_h^X sites will couple to z-polarized and σ^+ and σ^- excitation, respectively,[34] which indicates that the singlet interlayer exciton contains both IP and OP dipole and is consistent with Figure 3b. The zero DOP of IX_S is probably attributed to the scattering process of singlet to triplet states, as discussed above, which requires more investigation in the future. In contrast, both IX_T and IX_S show negligible DOP under high-power excitation (bottom panel of Figure 5c). We believe that the scattering process is one of the main reasons for the vanished DOP.[37] Please note that both IX_T and IX_S exhibit blue-shift under higher-power excitation in Figure 5a,c. The shift of peak position can be attributed to the repulsive dipole−dipole interaction. Exciton density increases under excitation with higher power, which enhances the dipole−dipole interaction and thus leads to blue-shift of the exciton peak.[38]

Utilizing the excitation power-tunable DOP, we designed an all-optical valley polarization switch, as shown in Figure 5d. Valley polarization switch indicates that the device has two states with distinct valley polarization, namely, high degree of valley polarization (ON state) and low degree of polarization (OFF state). The all-optical valley polarization switch is very stable within a few cycles with an on/off ratio up to 35. Table 1 summarizes the on/off ratio of several valley polarization switches in the existing literatures, and the on/off ratio of our device is an order of magnitude larger than reported values. The heterostructure without the SiO_2 cavity is also measured for comparison (Figure S8b), and such a valley polarization switch cannot be achieved. Therefore, we have demonstrated an optical and valley polarization switch based on the SiO_2 cavity-coupled heterostructure in an all-optical route with record on/off ratio, providing a new approach for the development of all-optical valley polarization switches.

Table 1. On/Off Ratio of Valley Polarization Switch

Heterostructure type	On/off ratio	References
WSe_2/WS_2	3.6	19
$WSe_2/MoSe_2$	∼2	12
WSe_2/WSe_2	6	39
$WSe_2/MoSe_2$	∼1	40
WSe_2/WS_2	35	This work

In summary, we report on the all-optical modulation IX_S and IX_T emission in a SiO_2 cavity-coupled TMDs heterostructure. The fine structure of the IX emission peak has been resolved benefiting from enhanced emission of IX_T. In addition, it is found that IX_T have a larger OP component thanIX_S via angle-resolved PL imaging, which leads to a stronger coupling between IX_T and the SiO_2 cavity and thus significantly enhances the IX_T emission. By using the selective enhancement of IX emission, an all-optical valley polarization switch with an on/off ratio of 35 has been demonstrated by utilizing the distinct valley polarization of IX_T emission. Our study provides a convenient and effective all-optical approach to investigate the fine structure of IX in TMD heterostructure and offers an alternative route to construct all-optical valleytronic devices.

MATERIALS AND METHODS

Sample Preparation. Monolayer WSe_2 and WS_2 flakes are mechanically exfoliated onto a 300 nm SiO_2/Si substrate in sequence to form a heterostructure with precise alignment. Both monolayers are identified by optical microscopy and confirmed by PL spectrum. Then, the SiO_2 spheres diluted in isopropyl alcohol are dropped on to the heterostructure, and SiO_2 spheres can be found sprayed on the heterostructure.

Optical Measurements. Low-temperature PL measurements are conducted in a temperature-controlled liquid nitrogen bath cryostat (sample in vacuum), and PL spectra are acquired on a home-built Raman spectrometer (Horiba, iHR-550). In the time-resolved PL measurements, we used a 78.1 MHz pulsed laser with 633 nm wavelength filtered from a supercontinuum light source (NKT Photonics, SuperK Fianium FIU-15) by using an acoustic−optic tunable filter (YSL Photonics, AOTF). The angle-resolved PL measurements were carried out on a home-built back focal plane momentum imaging system (Horiba, iHR320), and the numerical aperture of the collection objective lens is 0.9. SHG measurement is conducted under the excitation of a 780 nm fs laser.

ASSOCIATED CONTENT

Supporting Information

The Supporting Information is available free of charge at https://pubs.acs.org/doi/10.1021/acs.nanolett.3c01698.

Additional data on WGM modes of SiO_2 sphere, result of SHG measurement, detailed fitting curve, power-dependent PL of IX of $WSe_2/MoSe_2$ heterostructure, lifetime of singlet and triplet IX, schematic of angle-resolved PL setup, electric field simulation, IX emission of the heterostructure without a sphere under different excitation power, and DOP under right-hand circular excitation (PDF)

AUTHOR INFORMATION

Corresponding Authors

Xinglin Wen − *School of Optical and Electronic Information and Wuhan National Laboratory for Optoelectronics, Huazhong University of Science and Technology, Wuhan 430074, People's Republic of China*; orcid.org/0000-0002-8390-4456; Email: wenxl@hust.edu.cn

Dehui Li − *School of Optical and Electronic Information and Wuhan National Laboratory for Optoelectronics, Huazhong University of Science and Technology, Wuhan 430074, People's Republic of China*; orcid.org/0000-0002-5945-220X; Email: dehuili@hust.edu.cn

Authors

Yue Hu − *School of Optical and Electronic Information, Huazhong University of Science and Technology, Wuhan 430074, People's Republic of China*

Jiamin Lin − *Key Laboratory of Mesoscopic Chemistry, School of Chemistry and Chemical Engineering, Nanjing University, Nanjing 210093, People's Republic of China*

https://doi.org/10.1021/acs.nanolett.3c01698
Nano Lett. 2023, 23, 6581−6587

Wendian Yao − *School of Optical and Electronic Information, Huazhong University of Science and Technology, Wuhan 430074, People's Republic of China*
Yingying Chen − *School of Optical and Electronic Information, Huazhong University of Science and Technology, Wuhan 430074, People's Republic of China*
Junze Li − *School of Optical and Electronic Information, Huazhong University of Science and Technology, Wuhan 430074, People's Republic of China;* orcid.org/0000-0001-8837-5349
Sijie Chen − *School of Optical and Electronic Information, Huazhong University of Science and Technology, Wuhan 430074, People's Republic of China*
Lei Wang − *National Laboratory of Solid-State Microstructures, School of Physics, Nanjing University, Nanjing 210093, People's Republic of China*
Weigao Xu − *Key Laboratory of Mesoscopic Chemistry, School of Chemistry and Chemical Engineering, Nanjing University, Nanjing 210093, People's Republic of China;* orcid.org/0000-0002-3014-756X

Complete contact information is available at: https://pubs.acs.org/10.1021/acs.nanolett.3c01698

Author Contributions

X.L.W. and D.H.L. conceived the idea and supervised the project. Y.H. conducted the experiments and simulations. W.D.Y. helped on the data analysis. Y.Y.C., J.Z.L., and S.J.C helped with PL measurements and data interpretation. J.M.L, L.W., and W.G.X helped with SHG measurement and data analysis. All authors read and contributed to the revising of the manuscript.

Notes

The authors declare no competing financial interest.

■ ACKNOWLEDGMENTS

We acknowledge the support from National Key Research and Development Program of China (2022YFB2803900), National Natural Science Foundation of China (61674060, 62005091, 12074173), Natural Science Foundation of Jiangsu Province (BK20220121) and the Innovation Fund of WNLO.

■ REFERENCES

(1) Hu, Z. H.; Liu, X.; Hernandez-Martinez, P. L.; Zhang, S. S.; Gu, P.; Du, W.; Xu, W. G.; Demir, H. V.; Liu, H. Y.; Xiong, Q. H. Interfacial charge and energy transfer in van der Waals heterojunctions. *InfoMat* **2022**, *4* (3), e12290.
(2) Jiang, Y.; Chen, S. L.; Zheng, W. H.; Zheng, B. Y.; Pan, A. L. Interlayer exciton formation, relaxation, and transport in TMD van der Waals heterostructures. *Light Sci. Appl.* **2021**, *10* (1), 72.
(3) Liu, X.; Pei, J. J.; Hu, Z. H.; Zhao, W. J.; Liu, S.; Amara, M. R.; Watanabe, K.; Taniguchi, T.; Zhang, H.; Xiong, Q. H. Manipulating Charge and Energy Transfer between 2D Atomic Layers via Heterostructure Engineering. *Nano Lett.* **2020**, *20* (7), 5359−5366.
(4) Geim, A. K.; Grigorieva, I. V. Van der Waals heterostructures. *Nature* **2013**, *499* (7459), 419−425.
(5) Xu, W. G.; Liu, W. W.; Schmidt, J. F.; Zhao, W. J.; Lu, X.; Raab, T.; Diederichs, C.; Gao, W. B.; Seletskiy, D. V.; Xiong, Q. H. Correlated fluorescence blinking in two-dimensional semiconductor heterostructures. *Nature* **2017**, *541* (7635), 62−67.
(6) Rivera, P.; Schaibley, J. R.; Jones, A. M.; Ross, J. S.; Wu, S. F.; Aivazian, G.; Klement, P.; Seyler, K.; Clark, G.; Ghimire, N. J.; Yan, J. Q.; Mandrus, D. G.; Yao, W.; Xu, X. D. Observation of long-lived interlayer excitons in monolayer $MoSe_2$-WSe_2 heterostructures. *Nat. Commun.* **2015**, *6* (1), 6242.
(7) Tan, Q. H.; Rasmita, A.; Li, S.; Liu, S.; Huang, Z. M.; Xiong, Q. H.; Yang, S. A.; Novoselov, K. S.; Gao, W. B. Layer-engineered interlayer excitons. *Sci. Adv.* **2021**, *7* (30), eabh0863.
(8) Yu, H. Y.; Cui, X. D.; Xu, X. D.; Yao, W. Valley excitons in two-dimensional semiconductors. *Natl. Sci. Rev.* **2015**, *2* (1), 57−70.
(9) Mak, K. F.; Xiao, D.; Shan, J. Light-valley interactions in 2D semiconductors. *Nat. Photonics* **2018**, *12* (8), 451−460.
(10) Xu, X. D.; Yao, W.; Xiao, D.; Heinz, T. F. Spin and pseudospins in layered transition metal dichalcogenides. *Nat. Phys.* **2014**, *10* (5), 343−350.
(11) Wang, T. M.; Miao, S. N.; Li, Z. P.; Meng, Y. Z.; Lu, Z. G.; Lian, Z.; Blei, M.; Taniguchi, T.; Watanabe, K.; Tongay, S.; Smirnov, D.; Shi, S. F. Giant Valley-Zeeman Splitting from Spin-Singlet and Spin-Triplet Interlayer Excitons in $WSe_2/MoSe_2$ Heterostructure. *Nano Lett.* **2020**, *20* (1), 694−700.
(12) Ciarrocchi, A.; Unuchek, D.; Avsar, A.; Watanabe, K.; Taniguchi, T.; Kis, A. Polarization switching and electrical control of interlayer excitons in two-dimensional van der Waals heterostructures. *Nat. Photonics* **2019**, *13* (2), 131−136.
(13) Verzhbitskiy, I.; Vella, D.; Watanabe, K.; Taniguchi, T.; Eda, G. Suppressed Out-of-Plane Polarizability of Free Excitons in Monolayer WSe_2. *ACS Nano* **2019**, *13* (3), 3218−3224.
(14) Yu, H. Y.; Liu, G. B.; Yao, W. Brightened spin-triplet interlayer excitons and optical selection rules in van der Waals heterobilayers. *2D Mater.* **2018**, *5* (3), 035021.
(15) Sigl, L.; Troue, M.; Katzer, M.; Selig, M.; Sigger, F.; Kiemle, J.; Brotons-Gisbert, M.; Watanabe, K.; Taniguchi, T.; Gerardot, B. D.; Knorr, A.; Wurstbauer, U.; Holleitner, A. W. Optical dipole orientation of interlayer excitons in $MoSe_2$-WSe_2 heterostacks. *Phys. Rev. B* **2022**, *105* (3), 035417.
(16) Peimyoo, N.; Deilmann, T.; Withers, F.; Escolar, J.; Nutting, D.; Taniguchi, T.; Watanabe, K.; Taghizadeh, A.; Craciun, M. F.; Thygesen, K. S.; Russo, S. Electrical tuning of optically active interlayer excitons in bilayer MoS_2. *Nat. Nanotechnol.* **2021**, *16* (8), 888−893.
(17) Deilmann, T.; Thygesen, K. S. Interlayer Excitons with Large Optical Amplitudes in Layered van der Waals Materials. *Nano Lett.* **2018**, *18* (5), 2984−2989.
(18) Mak, K. F.; Shan, J. Opportunities and challenges of interlayer exciton control and manipulation. *Nat. Nanotechnol.* **2018**, *13* (11), 974−976.
(19) Ye, T.; Li, Y. Z.; Li, J. Z.; Shen, H. Z.; Ren, J. W.; Ning, C. Z.; Li, D. H. Nonvolatile electrical switching of optical and valleytronic properties of interlayer excitons. *Light Sci. Appl.* **2022**, *11* (1), 23.
(20) Joe, A. Y.; Jauregui, L. A.; Pistunova, K.; Valdivia, A. M. M.; Lu, Z. G.; Wild, D. S.; Scuri, G.; De Greve, K.; Gelly, R. J.; Zhou, Y.; Sung, J. H.; Sushko, A.; Taniguchi, T.; Watanabe, K.; Smirnov, D.; Lukin, M. D.; Park, H.; Kim, P. Electrically controlled emission from singlet and triplet exciton species in atomically thin light-emitting diodes. *Phys. Rev. B* **2021**, *103* (16), L161411.
(21) Wu, K.; Zhong, H. X.; Guo, Q. B.; Tang, J. B.; Zhang, J.; Qian, L. H.; Shi, Z. F.; Zhang, C. D.; Yuan, S. J.; Zhang, S. P.; Xu, H. X. Identification of twist-angle-dependent excitons in WS_2/WSe_2 heterobilayers. *Natl. Sci. Rev.* **2022**, *9* (6), nwab135.
(22) Andres-Penares, D.; Habil, M. K.; Molina-Sanchez, A.; Zapata-Rodriguez, C. J.; Martinez-Pastor, J. P.; Sanchez-Royo, J. F. Out-of-plane trion emission in monolayer WSe_2 revealed by whispering gallery modes of dielectric microresonators. *Commun. Mater.* **2021**, *2* (1), 52.
(23) Zhao, L. Y.; Shang, Q. Y.; Gao, Y.; Shi, J.; Liu, Z.; Chen, J.; Mi, Y.; Yang, P. F.; Zhang, Z. P.; Du, W. N.; Hong, M.; Liang, Y.; Xie, J. Y.; Hu, X. Y.; Peng, B.; Leng, J. C.; Liu, X. F.; Zhao, Y.; Zhang, Y. F.; Zhang, Q. High-Temperature Continuous-Wave Pumped Lasing from Large-Area Monolayer Semiconductors Grown by Chemical Vapor Deposition. *ACS Nano* **2018**, *12* (9), 9390−9396.
(24) Wang, G.; Robert, C.; Glazov, M. M.; Cadiz, F.; Courtade, E.; Amand, T.; Lagarde, D.; Taniguchi, T.; Watanabe, K.; Urbaszek, B.; Marie, X. In-Plane Propagation of Light in Transition Metal

Dichalcogenide Monolayers: Optical Selection Rules. *Phys. Rev. Lett.* **2017**, *119* (4), 047401.
(25) Choi, J.; Hsu, W.-T.; Lu, L.-S.; Sun, L.; Cheng, H.-Y.; Lee, M.-H.; Quan, J.; Tran, K.; Wang, C.-Y.; Staab, M.; Jones, K.; Taniguchi, T.; Watanabe, K.; Chu, M.-W.; Gwo, S.; Kim, S.; Shih, C.-K.; Li, X.; Chang, W.-H. Moiré potential impedes interlayer exciton diffusion in van der Waals heterostructures. *Sci. Adv.* **2020**, *6* (39), eaba8866.
(26) Zhang, L.; Gogna, R.; Burg, G. W.; Horng, J.; Paik, E.; Chou, Y. H.; Kim, K.; Tutuc, E.; Deng, H. Highly valley-polarized singlet and triplet interlayer excitons in van der Waals heterostructure. *Phys. Rev. B* **2019**, *100* (4), 041402.
(27) Aly, M. A.; Shah, M.; Schneider, L. M.; Kang, K.; Koch, M.; Yang, E. H.; Rahimi-Iman, A. Radiative pattern of intralayer and interlayer excitons in two-dimensional WS_2/WSe_2 heterostructure. *Sci. Rep.* **2022**, *12* (1), 6939.
(28) Li, W. J.; Lu, X.; Dubey, S.; Devenica, L.; Srivastava, A. Dipolar interactions between localized interlayer excitons in van der Waals heterostructures. *Nat. Mater.* **2020**, *19* (6), 624−629.
(29) Mahdikhanysarvejahany, F.; Shanks, D. N.; Muccianti, C.; Badada, B. H.; Idi, I.; Alfrey, A.; Raglow, S.; Koehler, M. R.; Mandrus, D. G.; Taniguchi, T.; Watanabe, K.; Monti, O. L. A.; Yu, H. Y.; LeRoy, B. J.; Schaibley, J. R. Temperature dependent moire trapping of interlayer excitons in $MoSe_2$-WSe_2 heterostructures. *npg 2D Mater. Appl.* **2021**, *5* (1), 67.
(30) Sun, X. Q.; Zhu, Y.; Qin, H.; Liu, B. Q.; Tang, Y. L.; Lu, T. Y.; Rahman, S.; Yildirim, T.; Lu, Y. R. Enhanced interactions of interlayer excitons in free-standing heterobilayers. *Nature* **2022**, *610* (7932), 478−484.
(31) Miller, B.; Steinhoff, A.; Pano, B.; Klein, J.; Jahnke, F.; Holleitner, A.; Wurstbauer, U. Long-Lived Direct and Indirect Interlayer Excitons in van der Waals Heterostructures. *Nano Lett.* **2017**, *17* (9), 5229−5237.
(32) Brotons-Gisbert, M.; Proux, R.; Picard, R.; Andres-Penares, D.; Branny, A.; Molina-Sanchez, A.; Sanchez-Royo, J. F.; Gerardot, B. D. Out-of-plane orientation of luminescent excitons in two-dimensional indium selenide. *Nat. Commun.* **2019**, *10* (1), 3913.
(33) Schuller, J. A.; Karaveli, S.; Schiros, T.; He, K. L.; Yang, S. Y.; Kymissis, I.; Shan, J.; Zia, R. Orientation of luminescent excitons in layered nanomaterials. *Nat. Nanotechnol.* **2013**, *8* (4), 271−276.
(34) Yu, H.; Liu, G.-B.; Yao, W. Brightened spin-triplet interlayer excitons and optical selection rules in van der Waals heterobilayers. *2D Mater.* **2018**, *5* (3), 035021.
(35) Schuller, J. A.; Karaveli, S.; Schiros, T.; He, K.; Yang, S.; Kymissis, I.; Shan, J.; Zia, R. Orientation of luminescent excitons in layered nanomaterials. *Nat. Nanotechnol.* **2013**, *8* (4), 271−276.
(36) Tang, Y.; Mak, K. F.; Shan, J. Long valley lifetime of dark excitons in single-layer WSe_2. *Nat. Commun.* **2019**, *10*, 4047.
(37) Surrente, A.; Klopotowski, L.; Zhang, N.; Baranowski, M.; Mitioglu, A. A.; Ballottin, M. V.; Christianen, P. C. M.; Dumcenco, D.; Kung, Y. C.; Maude, D. K.; Kis, A.; Plochocka, P. Intervalley Scattering of Interlayer Excitons in a $MoS_2/MoSe_2/MoS_2$ Heterostructure in High Magnetic Field. *Nano Lett.* **2018**, *18* (6), 3994−4000.
(38) Li, W.; Lu, X.; Dubey, S.; Devenica, L.; Srivastava, A. Dipolar interactions between localized interlayer excitons in van der Waals heterostructures. *Nat. Mater.* **2020**, *19*, 624−629.
(39) Liu, Y. D.; Dini, K.; Tan, Q. H.; Liew, T.; Novoselov, K. S.; Gao, W. B. Electrically controllable router of interlayer excitons. *Sci. Adv.* **2020**, *6* (41), eaba1830.
(40) Unuchek, D.; Ciarrocchi, A.; Avsar, A.; Sun, Z.; Watanabe, K.; Taniguchi, T.; Kis, A. Valley-polarized exciton currents in a van der Waals heterostructure. *Nat. Nanotechnol.* **2019**, *14* (12), 1104−1109.

https://doi.org/10.1021/acs.nanolett.3c01698
Nano Lett. 2023, 23, 6581−6587